Materials and Structures (2007) 40:553–566
DOI 10.1617/s11527-006-9162-4

ORIGINAL ARTICLE

Acoustic emission monitoring and numerical modeling of FRP delamination in RC beams with non-rectangular cross-section

A. Carpinteri · G. Lacidogna · M. Paggi

Received: 27 July 2005 / Revised: 8 February 2006 / Accepted: 9 March 2006 / Published online: 9 November 2006

Abstract A case study concerning both numerical modeling and in-situ monitoring of a retrofitted RC beam with non-rectangular cross-section is presented. Before retrofitting, non-destructive techniques, such as pull-out and impact tests, were used to estimate the mechanical parameters of concrete. At the same time, a long-term monitoring with the Acoustic Emission (AE) technique was carried out in order to investigate on creep effects and microcracking phenomena. Then, after a complete removal of the overload and retrofitting with FRP sheets, an in-situ loading test was performed. At that stage, the AE technique was again profitably used for the analysis of the cracking progression leading to FRP debonding. A numerical model of the structure is then proposed in the framework of the FE discretization with mechanical parameters estimated according to an inverse analysis on the monitored mechanical behavior of the structure before retrofitting. According to this model it is shown that, when the flexural inertia of the retrofitted beam is considerably higher than that of the unrepaired beam, snap-back instabilities can take place. Finally, considering the self-similarity between the acoustic emission phenomenon and seismicity, an analogy between the snap-back instability of the FRP delamination and that occurring during fault growth is proposed.

Résumé *Une étude de cas au sujet de modeler numérique et de surveiller in-situ d'un faisceau monté en rattrapage de RC avec la section transversale non-rectangulaire est présentée. Avant l'adaptation d'un faisceau, des techniques non destructives, telles que des essais à dégagement et à choc, ont été employées pour estimer les paramètres mécaniques du béton. En même temps, une surveillance à long terme avec la technique d'émission acoustique (AE) a été effectuée afin d'étudier sur des effets de fluage et des phénomènes de microfissuration. Puis, après un déplacement complet de la surcharge et l'adaptation ultérieure avec des feuilles de FRP, un essai in-situ de chargement a été réalisé. Á cette étape, la technique d'AE a été encore profitablement employée pour l'analyse de la progression de fissures menant au décollement du FRP. On propose alors un modèle numérique de la structure dans le cadre de la discrétisation FE avec des paramètres mécaniques estimés selon une analyse inverse sur le comportement mécanique surveillé de la structure avant l'adaptation ultérieure. Selon ce modèle, on le démontre que, quand l'inertie flexural du faisceau monté en rattrapage est considérablement plus haute que cela de la structure*

A. Carpinteri (✉) · G. Lacidogna · M. Paggi
Department of Structural Engineering and Geotechnics, Politecnico di Torino, Corso Duca degli Abruzzi 24, 10129 Turin, Italy
e-mail: alberto.carpinteri@polito.it

non réparé, les instabilités de snap-back peuvent avoir lieu. En conclusion, vu l'auto similarité entre le phénomène d'émission et la séismicité acoustiques, on propose une analogie entre l'instabilité de snap-back du décollement de FRP et cela qui se produit pendant la croissance de défaut.

Keywords RC bean strengthening · FRP delamination · Acoustic Emission Monitoring · Damage localization · Finite elements · Snap-back instability

1 Introduction

Structure rehabilitation is required whenever design mistakes, executive defects or unexpected loading conditions are assessed. In these cases, the use of a strengthening technique may be required in order to either increase the loading carrying capacity of the structure, or to reduce its deformations. The choice of the proper rehabilitation technique and the assessment of its performance and durability clearly represent an outstanding research point.

Considering steel-reinforced concrete beams, two typical problems requiring rehabilitation are: (i) too high deformations in service conditions and (ii) inadequate load carrying capacity.

In these cases, FRP sheets can be longitudinally bonded to the concrete members using epoxy adhesives. Since this repair method requires tension development of the sheet, the importance of the bond is widely recognized. In these retrofitted structures the main observed failure modes are [1–5]: (i) FRP debonding or concrete ripping at the ends of the beam, depending on the adhesive properties and (ii) FRP debonding in proximity of flexural cracks.

As a consequence, fracture parameters of the interface and the nonlinear behavior of concrete are expected to exert a key role in the effectiveness of the retrofitting procedure. This is particularly true when ultimate conditions are analyzed.

In the present paper we aim at characterizing the fracturing process leading to FRP delamination. In the early stages of damage, micro-cracking is a diffuse phenomenon which is difficult to be analyzed using traditional nondestructive techniques. Hence, from the experimental point of view, the main novelty of this study consists in the use of the AE technique to monitor the damage evolution in case of creep, and to analyze the micro-cracking due to FRP delamination.

From the numerical point of view, the proposed non-linear analysis developed according to the Finite Element discretization framework permits to focus on the effect of the non-rectangular cross-section on the delamination process. According to this model, it is shown that, when the flexural inertia of the retrofitted beam is considerably higher than that of the unrepaired beam, snap-back instabilities can take place. Finally, considering the self-similarity between the acoustic emission phenomenon and seismicity, an analogy between the snap-back instability of the FRP delamination and that occurring during fault growth is proposed.

2 The considered case study

The problem of FRP-strengthening of concrete beams subjected to high overloads is addressed. The examined beams sustain the roof of a school which rises in an urban area close to Turin, in the northern part of Italy. This single story building was erected in 1974, covering a rectangular area of 24×30 m^2. The beams have a reversed V cross-section (see Fig. 1) and are disposed along the major direction of the building. They are simply supported on concrete columns with a span length of 14.4 m.

The self-weight of the roof slabs is transmitted to the beams through vertical concrete walls. Since these walls are close to each other with an interaxis of 1.8 m, it is possible, from an engineering point of view, to substitute the concentrated loads with an equivalent pressure distribution.

2.1 Mechanical tests

Mechanical tests have been applied to characterize the constituent materials. Pull-out and impact tests have been performed to make an in-situ

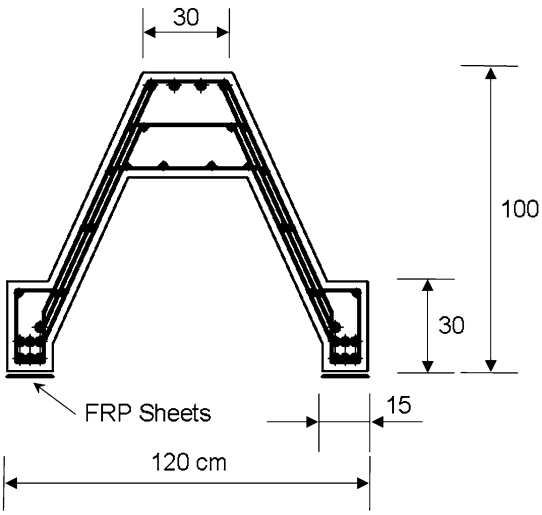

Fig. 1 Scheme of the beam cross-section

estimation of the compressive strength R_{ck} and of the elastic modulus E_c of concrete.

The pull-out test consists in pulling out a metal insert embedded in the concrete mass and measuring the exerted pulling force. According to this method, it is possible to estimate the average concrete compressive strength using correlation formulae available in the Literature. The electronic testing apparatus has been provided by the 4 EMME Service S.p.a. company from Bolzano, Italy. By performing a set of 10 pull-out tests in different regions of the beams, an average concrete compressive strength of 35 MPa has been estimated.

In addition, impact tests have been carried out in order to have an independent estimation of the concrete compressive strength. Using the test apparatus by SEB S.r.l. from Milano, Italy, we have estimated $R_{ck} = 50$ MPa from the tests performed over the tensile regions of the beams and $R_{ck} = 40$ MPa from the compressed regions. As expected, both measures differ form the value computed according to pull-out tests due to boundary effects such as clusters of aggregates or steel reinforcement close to the tested external surface. Namely, a low value of the steel cover of 20 mm justifies the higher value of R_{ck} in the tensile zones of the beam characterized by a high steel density. In any case, since the computed values of R_{ck} have a low dispersion, the impact test results indicate that the concrete properties are almost uniform throughout the whole structural elements.

2.2 AE testing apparatus and long-term monitoring

A long-term monitoring of the mid-span deflection of the beam has been performed under in-situ loading conditions. They consist in the weights of the covering slabs and of the beam for a total amount of 60 kN/m distributed along the whole beam length. After 4,486 h of monitoring, a mid span deflection of 37 mm has been observed. It has to be noticed that this maximum deflection is higher than that expected according to the elastic analysis performed on the uncracked beam. Creep effects are a possible explanation to this mechanical behavior [6].

Hence, the AE technique has been used during the long-term monitoring in order to analyze the time evolution of microcracking phenomena. According to this technique, it is possible to detect the onset and the evolution of stress-induced cracks. Crack opening, in fact, is accompanied by the emission of elastic waves which propagate within the bulk of the material. These waves can be detected and recorded by transducers applied to the surface of the structural elements.

AE monitoring is performed by means of piezoelectric (PZT) sensors, using crystals that give out signals when subjected to a mechanical stress, Fig. 2. The amplitude of the elastic pressure waves, which varies from one material to another even by orders of magnitude, is usually very weak, less than a millionth (10^{-6}) of the atmospheric pressure. Accordingly, the electric signals emitted by the transducers have to be greatly amplified (10^4 or 10^5 times) before they can be processed [7–14].

The signal from the transducers is preamplified, converted into electric voltage and then filtered to eliminate unwanted frequencies, such as the vibrations due to the mechanical instrumentation, which are generally lower than 100 kHz.

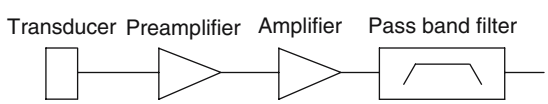

Fig. 2 Acoustic Emission measurement system

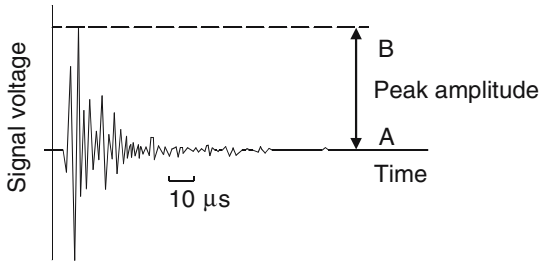

Fig. 3 Example of AE signal identified by the transducer

Up to this point the signal can be represented as a damped oscillation, Fig. 3. The AE signals collected during the experimentation are usually composed of thousands of such damped oscillations. Therefore, the signals are analyzed by a threshold measurer which counts the oscillations exceeding a predetermined voltage level, measured in volt (V).

This method of analysis is called Ring-Down Counting (RDC) and is widely used for the identification of defects with the AE technique [11, 12]. The counting number of oscillations, N, can be assumed to be directly correlated to the quantity of energy released during the loading process. Furthermore, it has been experimentally shown that the corresponding increments, ΔN, increase proportionally to the crack length. Clearly, this hypothesis is correct in the case of slow-crack growth [9].

With this method it is possible to define a *single event* as the amount of oscillations, over a specified threshold, produced by a single AE signal or by a group of signals in a given time interval (see Fig. 4) [10].

The long-term monitoring equipment adopted in this study consists in 4 ATEL® units provided of PZT resonant transducers, calibrated on inclusive frequencies between 100 kHz and 400 kHz, and control units, fitted with a built-in threshold level measurer, a recorder and an oscillation counter. The system does not provide the complete waveform of transient data. This equipment permits to perform a parameter-based analysis according to the RDC method [15]. This approach is very well suited for long-term monitoring, since it permits to handle with a reasonable quantity of data [14].

The threshold level for the signals recorded by the equipment, fixed at 100 μV, is amplified up to

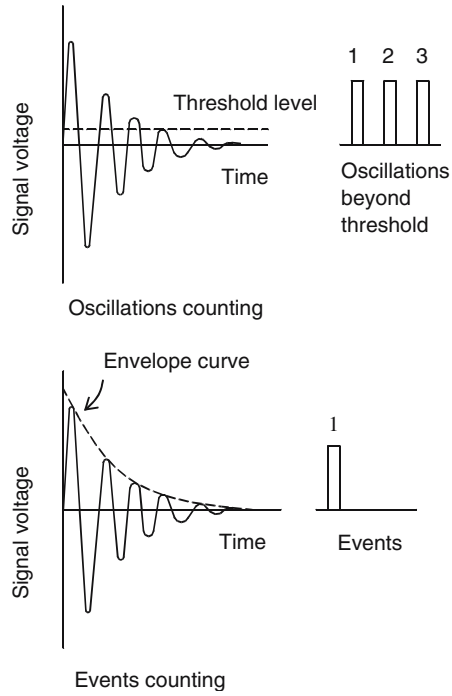

Fig. 4 Counting methods used in the AE technique

100 mV. The amplification gain, given by the relationship $\mathrm{dB} = 20\log_{10} E_u/E_i$, where E_u/E_i is the ratio between the output voltage and the input voltage, turns out to be equal to 60 dB. This is the value of signal amplification generally adopted in monitoring AE events in concrete [10]. The oscillation counting limit has been fixed at 255 oscillations every 120 s of signal recording [7–9]. In this way, a single event is the result of 2 recorded minutes.

From the Literature it is know that the duration of a signal emitted during cracking of a non-metallic material, like concrete, is around 2,000 μs and that the amplitude of a direct non-amplified signal is of the order of 100 μV [16]. Hence, considering the attenuation phenomena intercurring in the travel path between the source of the signal and the location of the sensor, it can be assumed that the measuring system is able to detect the most relevant AE events reflecting the cracking process of the material. Attenuation properties, in fact, depend on the frequency range and higher frequency components propagate in concrete with a greater attenuation. Based on experimental results, for a measuring area at a

distance of 10 m from the sensor, only AE waves with frequency components lower than 100 kHz are detectable, Fig. 5 [10].

Considering the attenuation properties typical of concrete, three AE transducers have been positioned along the tensile region of the beam: one in correspondence of the middle of the beam and the others symmetrically positioned at 1/3 of the total span from the supports. In this way, the relative distances between the transducers and the distance from the beam ends and the neighborhood sensors inside the beam have been reduced in the range 2.4–4.8 m.

Concerning the transducer positioned in the middle of the beam, the AE counting number and the AE event rate are shown in Fig. 6 as functions of time. Similar trends have been recorded by the other transducers. However, in these lateral positions, the total counting number is approximately equal to 1/4 of that observed in the mid-span position.

From Fig. 6 it is possible to recognize that the energy release, quantified in terms of AE events with amplitude higher than 100 μV, is not a continuous phenomenon but it regularly occurs at discrete times [17].

According to the Literature, two possible explanations of this behavior are: (i) the stress state is higher than one half of the material strength and (ii) the deformation of the structural element increases vs. time.

During the monitoring period, under constant applied loads, an increment of the structural deformation has been noticed, with an increase of the mid-span deflection of around 5 mm. Hence,

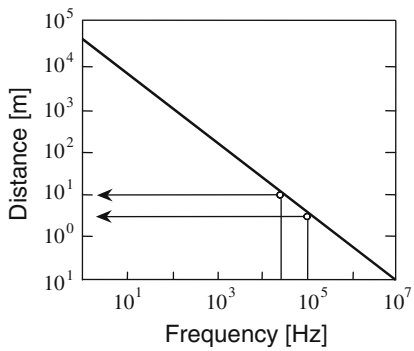

Fig. 5 Relationship between the signal detection distance and the signal frequency in the AE technique

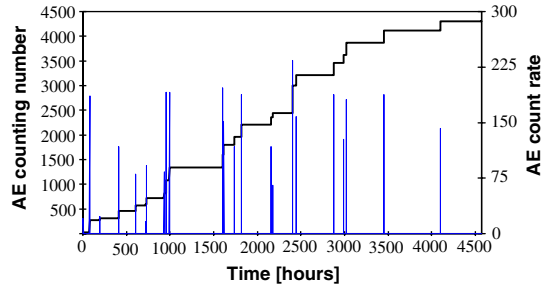

Fig. 6 Results of AE monitoring with the ATEL® equipment. The diagram represents the AE counting number and the AE count rate (measured over 120 s) vs. time

the energy release has to be ascribed to creep effects which are responsible for the microcracking process detected by the AE transducers.

3 Retrofitting with FRP sheets

To improve the loading carrying capacity and reduce the effects of microcracking, the beams have been externally reinforced with FRP sheets after a preliminary complete removal of the existing overload. Two carbon fiber sheets having a 1.4 mm thickness, 100 mm width and Young's modulus of 240 MPa have been bonded along the whole beam length using an epoxy adhesive.

3.1 In-situ loading test of the retrofitted beams

In order to evaluate the loading carrying capacity of the retrofitted beams, an in-situ loading test of a retrofitted beam has been carried out. The load has been applied by filling 16 vessels with water. Since each vessel has a capacity of 1,000 l, a total vertical load of 160 kN has been applied. The vessels have been symmetrically positioned with respect to the center of the beam, covering a loading area of $4.00 \times 2.40 = 9.60$ m^2 (see Fig. 7). Gradually filling the vessels, four loading steps of 40 kN per step have been applied. After each step, the applied load was kept constant for 10 min. The whole loading test last approximately 3 h. A monitored mid-span deflection of 11 mm has been observed at the end of the loading test.

Fig. 7 Photo of the loading apparatus. Circles denote the positions of the attached ATEL® AE transducers. Transducer No. 1 is on the left

3.2 AE monitoring and damage localization

During the loading test, 4 AE ATEL® transducers have been positioned in order to investigate on the effect of the external reinforcement on the flexural crack growth and on the progress of the FRP-concrete debonding phenomenon (see the *circles* in Fig. 7 denoting the sensors locations).

The full flexural capacity of the FRP-sheets has not been reached at the end of the test, since a macroscopic delamination has not been seen. On the other hand, flexural cracks have been observed in the middle of the beam and at 1/3 of the total span from the right support.

Adopting the RDC method, time evolution of the AE counting numbers detected by the AE transducers is shown in Fig. 8.

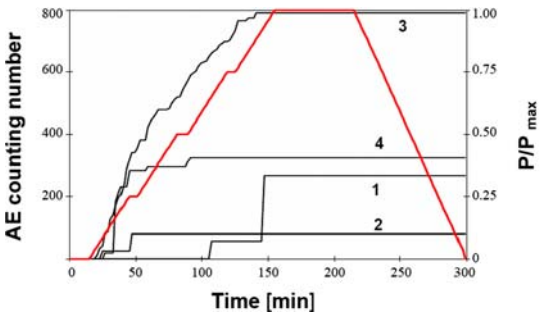

Fig. 8 AE activity during the loading test (ATEL® sensors). Transducer No. 1 is positioned at the beam end; transducer No. 4 is placed in the middle of the beam. The others are in intermediate positions. Loading evolution is also reported. P and P_{max} denote the applied load at a given time and the maximum load reached at the end of the test

Transducers No. 3 and 4 are close to the flexural cracks and begin to detect acoustic emissions from the very beginning of the loading test. At the end, they have detected the highest number of acoustic emissions, followed by the transducer No. 1, close to the beam support. It is important to notice that acoustic events are not detected by the transducer No. 1 for vertical loads lower than 80 kN. This result is in agreement with the typical progression of cracking and collapse of retrofitted beams (see Fig. 9). Flexural cracks propagate upwards as loading progresses, but remain very narrow throughout the loading history. Delamination of the FRP sheets together with a thin layer of concrete takes place only when shear cracks develop close to the support. The progress of the acoustic events observed in our loading test is then in agreement with that expected from the typical cracking progression developing in these reinforced structures.

In addition, a more accurate localization of the AE sources along the beam has been put forward using a more sophisticated AE acquisition system.

This equipment adopted by the Authors consists of six USAM® units synchronized for multichannel data processing. This system permits to perform a signal-based acoustic emission analysis using the complete waveform of transient data, as described in [14]. Each unit contains a preamplified broadband PZT sensor sensitive to the

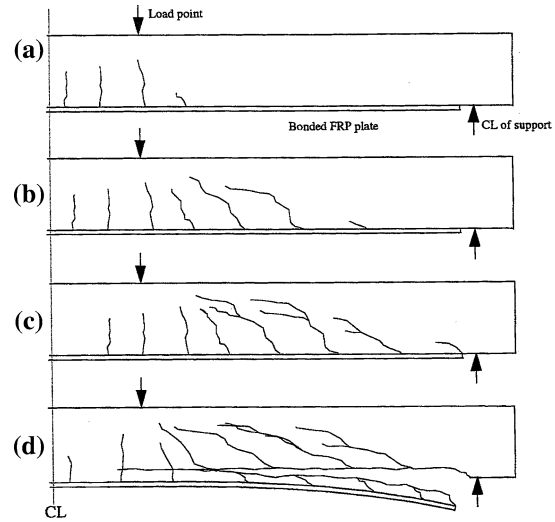

Fig. 9 Typical progression of cracking and collapse for a FRP retrofitted beam (reprinted from [18])

frequency range between 50 kHz and 800 kHz. The most relevant parameters acquired from the signals (arrival time, amplitude, duration, and number of oscillations) are stored in the USAMs memory and simultaneously downloaded into a PC for a multi-channel data processing.

The AE source location can be deduced using the difference among the first P-wave arrival times at each of the AE transducers. Using this equipment it is usually assumed that the amplitude threshold of 100 μV of the non-amplified signal is appropriate to distinguish between the P-waves and the S-waves arrival times. In fact, the P-waves are usually characterized by a higher amplitude of the signal [16, 19–21]. In RC beams the velocity of P-waves is usually anisotropic. P-wave velocity in each direction is different from the mean value with a variation of approximately 20%. Therefore, according to the suggestions in [16], the localization of the source points can be treated as a least-squares problem in which the propagation velocity is not assumed a priori, but is included in the problem unknowns. From this computation, the localization of microcracks is performed and the condition of the monitored specimen can be determined. Moreover, the error in the AE source location is estimated close to ±10 mm, according to our previous experimental analyses [22]. See also [16, 23] for more detailed procedures about the error computation.

The USAM® sensors have been placed on the opposite side of the beam at symmetric positions with respect to those of the sensors ATEL®, see Fig. 10.

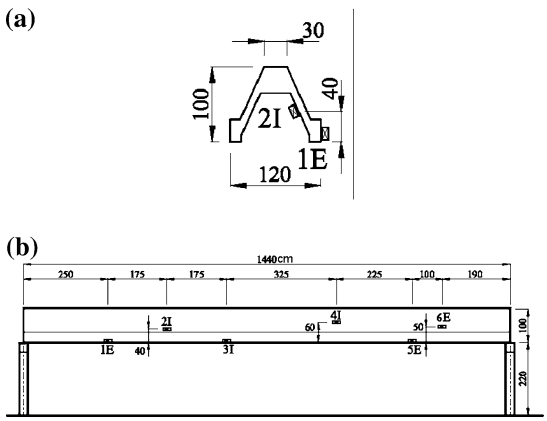

Fig. 10 (**a**) Beam cross-section indicating the position of the USAM® transducers. The ATEL® transducers are applied on the opposite side. (**b**) Lateral view of the beam indicating the positions of the six USAM® transducers

According to this approach, the AE source points are determined and depicted in Fig. 11b with black points.

From the post-processing of the AE signals used for the localization we have observed that their frequencies range from 60 kHz to 120 kHz, whereas the average propagation velocity in concrete appears to be of 1,500 m/s.

Analogous trends concerning the total number of AE events vs. time have been recorded by both the sensor types, suggesting the occurrence of the same evolution of the cracking process along the two FRP sheets.

4 Numerical analysis of concrete-FRP delamination

A three-dimensional finite element model of the whole beam is proposed in order to investigate on the propagation of the FRP-concrete delamination. A bilinear cohesive law is adopted for the description of the non-linear interface behavior, as suggested in provision codes and in recent research studies [24–28] (see a sketch of the adopted cohesive law and the corresponding parameters in Fig. 12).

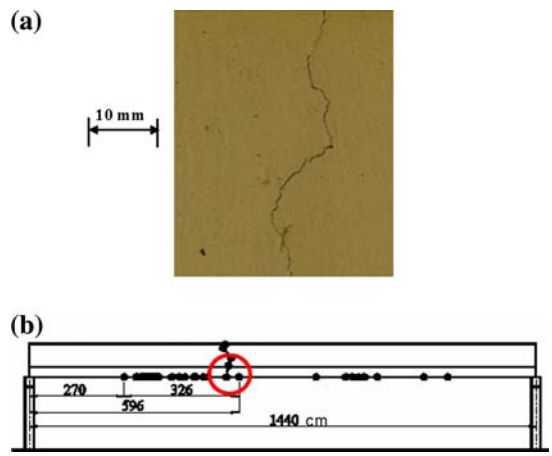

Fig. 11 (**a**) Photo of a portion of the flexural crack in between the transducers No. 2 and No. 3. The circle indicates the photographed area. (**b**) Lateral view of the beam showing the localized AE sources by the USAM® equipment

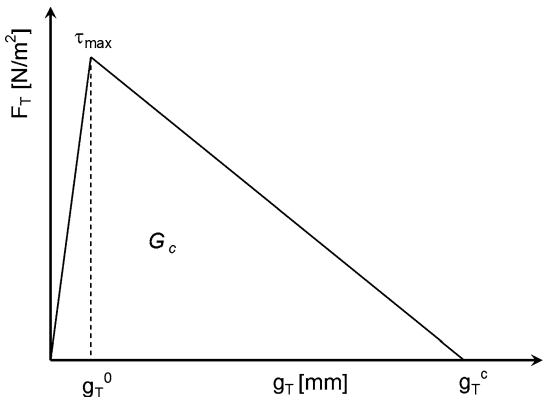

Fig. 12 Parameters of the bilinear cohesive model

Two different values of the Mode II interface fracture energy G_c have been considered. The former, corresponding to a FRP–concrete delamination at the interface, is equal to 300 N/m and it is obtained by setting $g_T^c = 200\mu m$, $g_T^0 = 1\mu m$ and $\tau_{max} = 3$ MPa, according to the recommendations in [24–26]. The latter is 30 N/m, simulating a delamination of the FRP sheet together with a thin layer of the concrete cover, i.e. the phenomenon usually referred to as concrete ripping [18]. As a first approximation, since we are mainly interested in the analysis of the growth and stability of the delamination process (stages (c) and (d) in Fig. 9), concrete is assumed to behave linear elastically and only the non-linear behavior of the interface is retained in the model.

Further developments of the present study could concern the study of the crack patterns in the stages (a)–(c) considering a non-linear constitutive law also for concrete.

The concrete Young's modulus has been estimated according to an inverse analysis on the deformation behavior of the beam experimentally monitored before retrofitting. From pull-out tests performed on the beams it is possible to correlate the concrete Young's modulus to the characteristic compressive strength R_{ck} of concrete using correlation formulae as discussed in [29]. According to this method, the estimated Young's modulus is 34 GPa.

Using this value, a preliminary three-dimensional FE simulation of the whole beam without FRP sheets and subjected to the overloads characteristic of the long-term monitoring has been carried out. The predicted mid-span deflection is then equal to 28 mm, which is lower than that experimentally monitored (37 mm).

As also noticed in the previous section, this difference can be ascribed to creep and micro-cracking that increase the overall deformation of the beam compared to the same structure without time-dependent phenomena. Hence, in order to take into account these effects, an effective value of the Young's modulus $E_c = 24$ GPa is used in the subsequent FE analyses instead of the nominal one estimated through pull-out tests. This approach is consistent with the linear theory of creep suggesting that, as a first approximation, the effect of creep on the deformation can be taken into account by reducing the nominal Young's modulus of concrete. In this way, the numerically predicted mid-span deflection matches exactly the experimental value.

Concerning the simulation of the loading test performed on the FRP-retrofitted beam, numerical predictions and experimental observations are compared in the load vs. mid-span deflection diagram in Fig. 13, with an error less than 1%.

It has to be noticed that computations with different values of the Mode II fracture energy (30 N/m and 300 N/m) predict almost the same results. In the considered loading range, in fact, micro-slips between FRP and concrete are not high enough to produce delamination. This is also experimentally confirmed by AE transducers that have detected the progress of cracking leading to

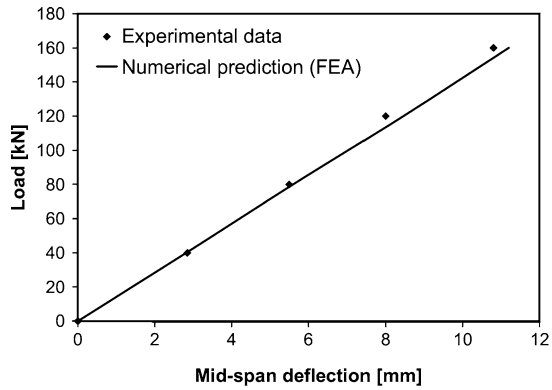

Fig. 13 Load vs. mid-span deflection: comparison between FE predictions and experimental monitoring

the onset of debonding only (stages (a)–(c) in Fig. 9).

The applied load is then numerically increased above 160 kN in order to study the evolution of the debonding process (stages (c)–(d) in Fig. 9). Assuming G_c = 30 N/m, delamination firstly initiates in correspondence of the simple support at the FRP-cutoff point when the external load reaches 320 kN. Then, delamination propagates towards the mid-span position (see Figs 14, 15).

Interestingly, the delamination process does not evolve symmetrically with respect to the middle of the beam, although both geometric and loading conditions are symmetric. This behavior is due to different boundary conditions imposed at the ends of the beam. In fact, in order to match the real in-situ boundary conditions, the nodes

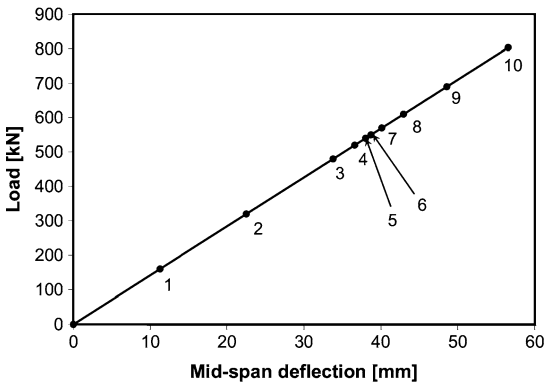

Fig. 14 Load vs. mid-span deflection for the numerical simulation of the delamination process

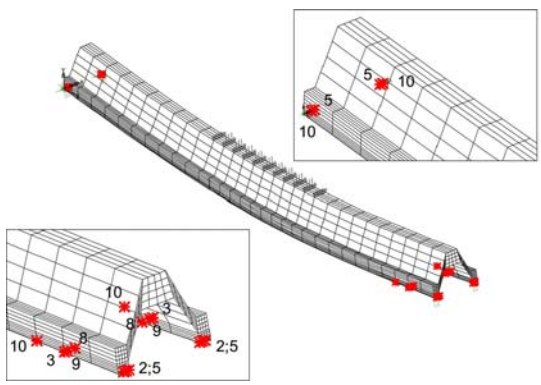

Fig. 15 Numerical simulation of the delamination process: star marks denote delamination points. The numbers from 2 to 10 correspond to different loading levels, as reported in Fig. 14

along the right-end side of the beam are simply constrained against vertical displacements. On the contrary, the base nodes at the opposite extreme are fixed against vertical, lateral and longitudinal displacements, due to the presence of a border transversal beam. As a result, micro-slips along the concrete-FRP interface are higher at the right end of the beam than those at the opposite side.

Moreover, it has to be remarked that, under vertical loads, the beam manifests not only vertical and longitudinal displacements, but also lateral (along the x-coordinate) deformations, due to its characteristic cross-section. In fact, during loading, the flanks of the beam tend to laterally expand with respect to the vertical symmetry line. As a result, these displacements can contribute to debonding.

Due to the herein proposed 3D model, lateral and longitudinal displacements promoting delamination can be quantified and compared. Contour plots of longitudinal and lateral displacements are shown, respectively, in Figs. 16 and 17 for a vertical load equal to 160 kN, that is at the end of the experimental loading test.

Both displacements have a non-symmetric distribution along the beam. The maxima are located in correspondence of the right-end of the beam and are equal to $\delta_z \cong$ 2.3 mm and $\delta_x \cong$ 0.7 mm. Hence, as expected, lateral displacements are lower than the longitudinal ones. Nevertheless, they have the same order of magnitude and therefore provisional codes should pay attention to their effect for this type of cross-sections. Moreover, it has to be noticed that the load corresponding to the onset of delamination at the right-end side is far lower than that needed for debonding at the opposite side (320 kN vs. 540 kN, as shown in Fig. 14). Hence, it seems that the higher the degree of constraint, the higher is the critical load for the onset of debonding.

Finally, analyzing the overall mechanical response of the structure, it is possible to observe that, since the flexural inertia of the retrofitted beam is similar to that of the unrepaired structure, the load vs. mid-span deflection curve still remains almost linear during delamination.

On the other hand, a completely different mechanical response is expected when the

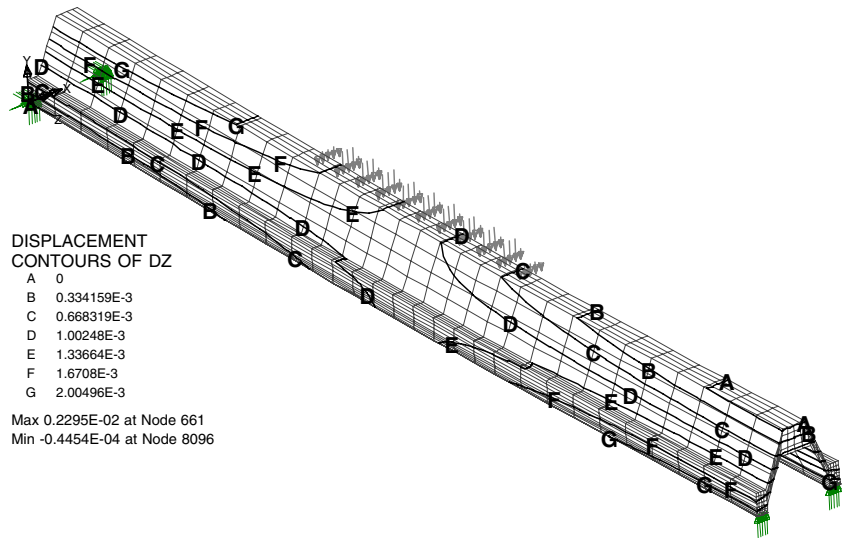

Fig. 16 Contour plot of longitudinal displacements (along the z-coordinate) of the whole beam. This diagram corresponds to a total applied load of 160 kN, i.e. at the end of the loading test

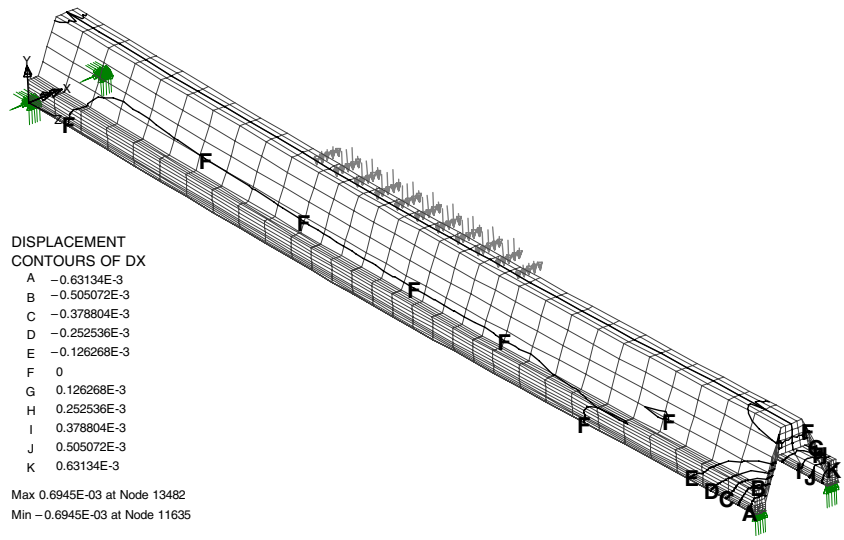

Fig. 17 Contour plot of lateral displacements (along the x-coordinate) of the whole beam. This diagram corresponds to a total applied load of 160 kN, i.e. at the end of the loading test

flexural inertia of the retrofitted beam is significantly higher than that of the concrete beam before retrofitting. This case can be due to a large amount of used fibers or for beams having significant creep effects and flexural cracks. In such conditions, when delamination takes place, an unstable interface crack propagation occurs, thus resulting in a sharp snap-back branching.

A numerical simulation of this brittle mechanical response is proposed in Fig. 18 with superimposed experimental data of four-point bending tests on repaired RC beams by David et al. [30, 31] (see the loading scheme sketched in Fig. 9). Mechanical parameters for this case study are reported in [31], whereas the Mode II fracture energy has been set equal to G_c = 50 N/m. In order to analyze the evolution of the debonding process, the arc-length control method has been adopted in the numerical scheme.

According to this approach, it is shown that both the external load and the mid-span deflection of the beam have to be reduced during crack propagation in order to have a uniform monotonic increase of the interface crack length (see Fig. 18) [32]. This result is in agreement with experimental tests performed under displacement

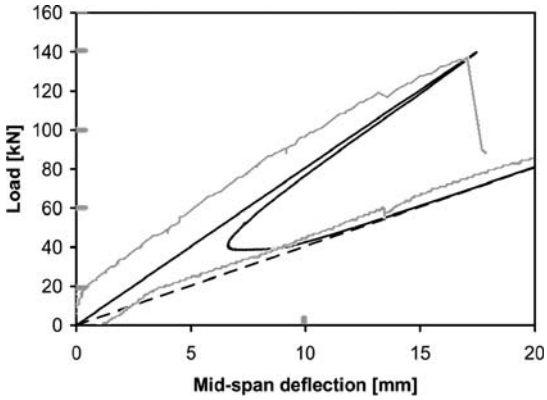

Fig. 18 Comparison between the numerically predicted snap-back curve (*solid line*) and the experimental results from [30] (*gray line*). The dashed line corresponds to the numerically predicted behavior of the unrepaired concrete beam

control in [30] which clearly show the occurrence of a sudden structural failure as soon as the interface crack propagates and separates the concrete cover bonded to the FRP sheets from the rest of the beam. After complete delamination, the stiffness of the structure equals that of the unrepaired material, reported with dashed line in the same diagram.

5 Analogy between FRP delamination and fault growth instabilities

The monitoring of acoustic emission has proven to be one of the more powerful tools available for analyzing brittle fracture. In seismicity this technique is used to determine the spatial and temporal variations in microcracking during sample deformation. Hence, from the arrival times of acoustic signals, event hypocenters can be determined [16, 19, 20, 23]. Most AE event location studies have been devoted to the search for clustering patterns which would indicate the onset of fault nucleation. Moreover, numerous studies have also confirmed that AE event amplitudes obey the power law frequency–magnitude relation observed for earthquakes.

Experimental studies on the fracture of brittle rocks show the tendency for fault growth to proceed in a sudden, uncontrolled manner after fault initiation. Lockner et al. [23] have performed

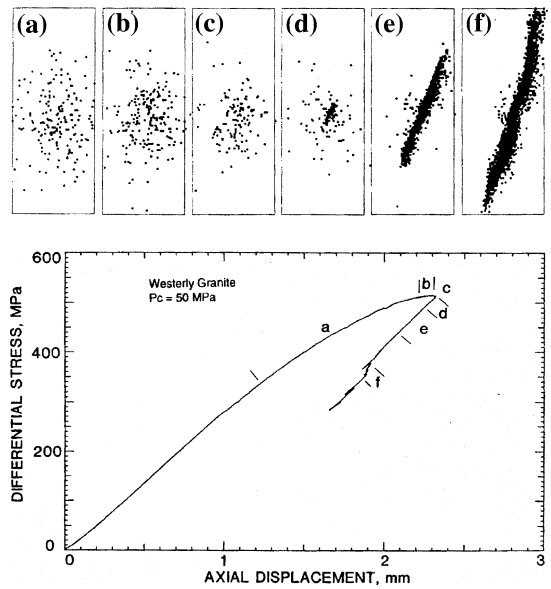

Fig. 19 Differential stress vs. axial displacement for a triaxial compression test of Westerly granite. Sample dimensions: 76.2 mm diameter and 190.5 mm height. The progression of the AE source locations is shown in the pictures (**a**) to (**f**) (reprinted from Lockner [23])

triaxial compression tests on cylinders of intact Westerly granite, demonstrating the instability of fault growth. This behavior is shown in Fig. 19, where the acoustic emission hypocentral locations during fault formation and growth are depicted. The fault plane clearly appears as a diagonal failure at the steps (d)–(f). The corresponding stress–displacement curve shows the occurrence of a snap-back instability and indicates segments of the experiments from which acoustic emission plots are made.

This unstable behavior suggests a direct analogy with the FRP delamination process, since in both situations the crack pattern leads to critical snap-back instabilities in the overall response. In the FRP systems the snap-back branch can be experimentally captured only if the loading process is controlled by a monotonic increasing function of time, e.g. the interface crack length. Similarly, during fault growth the post-peak behavior was captured by Lockner et al. [23] by controlling the axial stress to maintain a constant rate of acoustic emission, i.e. by controlling the fault length.

From AE events it is possible to compute the slope of the frequency–magnitude Richter's

relation for earthquakes, defined by $\log N = a - bM$, where N is the number of earthquakes larger than magnitude M and a and b are constants. Analyses of earthquakes foreshocks have revealed precursory variations in b which decreases to a minimum at the time of fault nucleation. This behavior was quantified by Lockner et al. [23] by analyzing the AE data for the triaxial compression tests on cylinders of intact Westerly granite whose unstable behavior is shown in Fig. 19. In this case a decrease in the b-values from 2.3 to 1.1 was noticed during the stages of pre-nucleation, i.e. from stage (a) to (d) in Fig. 19.

Along the lines of the earthquake seismology, the magnitude in terms of the AE technique is defined as follows: $M = \log A_{\max} + f(r)$, where $A_{\max}$ is the signal amplitude, measured in microvolts, while $f(r)$ is a correction factor taking into account that the amplitude of the signal is a decreasing function of the distance r between the source and the sensor. Therefore, according to Uomoto [33], the amplitude reduction of the AE signals in large-sized concrete structures is $f(r) = k\,r$. The parameter r is measured in meters and k is equal to five magnitudes per meter. In order to follow this procedure, the signal amplitude analyses must be performed by means of the USAM® equipment that is able to identify the complete shape of AE waves.

By performing a similar post-processing on the AE signals recorded during the loading test of the retrofitted FRP beam, the b-value corresponding to the maximum external load was approximately equal to 1.4. According to this analogy, the computed b-value higher than 1.1 suggests that the cracking process corresponds to an intermediate situation between stages (a) and (c) in Fig. 9. This remark, which is in good agreement with the laboratory tests performed by Colombo et al. [34] on RC beams, is also recognized in our experimental observation of the crack pattern.

6 Conclusions

An in-situ loading test on a retrofitted RC beam has been proposed. On the basis of the AE monitoring, the cracking progression leading to FRP delamination has been detected and analyzed. The proposed experimental procedure permits to correlate the evolution of the acoustic events with the progress of cracking leading to delamination. Moreover, using a localization procedure, the sources of acoustic events can be detected. These results imply that the AE technique can be profitably applied not only to the non-destructive monitoring of concrete and masonry structures [7], but also to the characterization of the debonding process in bi-material structural components.

Furthermore, using a 3D FE model, the stability of the delamination process has been investigated and interpreted. In this stage, the analysis has focused on the effect of the non-linear behavior of the interface on the structural response. Hence, the evolution of the crack pattern leading to delamination has not been modeled. This simplification which makes the problem treatable provides structural predictions consistent with experimental data when pure delamination/concrete ripping is the actual failure mode (see the good agreement with experimental data in Fig. 18).

On the other hand, local debonding phenomena along the beam caused by flexural cracks cannot be investigated with our proposed model and further studies should be put forward in this direction in order to fully characterize the problem.

In any case, it has been clearly demonstrated that, when the flexural inertia of the repaired structure is considerably higher than that of the unrepaired beam, snap-back instabilities can take place, thus resulting in significant change from a ductile to a brittle mechanical structural response [32].

Finally, thanks to the 3D FE model, it has been shown that the non-compact geometry of the considered cross-section is responsible for lateral displacements that have the same order of magnitude as the longitudinal ones. Moreover, it has been shown that the degree of constraint can significantly affect the critical load corresponding to the onset of delamination.

Both aspects are worth being investigated by the Scientific Community in order to propose new prescriptions for provisional codes. Finally, the analogy between the instabilities during FRP delamination and fault growth have been put into

evidence. This suggests the possibility to interpret the stability of both behaviors according to the well-known Richter–Gutenberg frequency–magnitude relation for earthquakes.

Acknowledgements Support of the Ministry of University and Research (MIUR) is gratefully acknowledged. The Authors would like to thank the Ph.D. student Gianni Niccolini for the elaboration of the AE sources location and the Architects Massimo Aprile and Luigi Bacco for the technical support provided in the structural monitoring.

References

1. Leung CKY (2004) Delamination failure in concrete beams retrofitted with a bonded plate. J Mater Civil Eng 13:106–113
2. Leung CKY (2004) Fracture mechanics of debonding failure in FRP-strengthened concrete beams. In: Li VC, Leung CKY, Willam KJ, Billington SL (eds) Proc. of 5th Intern. Conf. on Frac. Mech. of Concr. and Concr. Struct. (FraMCoS-5), Vail, Colorado, USA 1, pp 41–52
3. Alaee FJ, Karihaloo BL (2003) Fracture model for flexural failure of beams retrofitted with CARDIFRC. ASCE J Eng Mech 129:1028–1038
4. Taljsten B (1997) Strengthening of beams by plate bonding. ASCE J Mater Civil Eng 9:206–212
5. Arduini M, Di Tommaso A, Nanni A (1997) Brittle failure in FRP plate and sheet bonded beams. ACI Struct J 94:363–370
6. Carpinteri A, Lacidogna G, Pugno N (2005) Creep monitoring in concrete structures by the acoustic emission technique. In: Proc. of the 7th Int. Conf. on creep, shrinkage and durability of concrete and concrete structures (Concreep7), Nantes, 12–14 September 2005
7. Carpinteri A, Lacidogna G, Pugno N (2004) Damage diagnosis and life-time assessment of concrete and masonry structures by an acoustic emission technique. In: Li VC, Leung CKY, Willam KJ, Billington SL (eds) Proc. of 5th Int. Conf. on Frac. Mech. of Concr. and Concr. Struct. (FraMCoS-5), Vail, Colorado, USA 1, pp 31–40
8. Carpinteri A, Lacidogna G, Pugno N (2004) A fractal approach for damage detection in concrete and masonry structures by the acoustic emission technique. Acoust Tecn 38:31–37
9. Carpinteri A, Lacidogna G (2006) Damage monitoring of an historical masonry building by the acoustic emission technique. Mater Struct (in press)
10. Ohtsu M (1996) The history and development of acoustic emission in concrete engineering. Mag Conc Res 48:321–330
11. Pollock AA (1973) Acoustic emission-2: acoustic emission amplitudes. Non-Destruct Test 6:264–269
12. Brindley BJ, Holt J, Palmer IG (1973) Acoustic emission-3: the use of ring-down counting. Non-Destruct Test 6:299–306
13. Holroyd T (2000) The acoustic emission and ultrasonic monitoring handbook. Coxmoor Publishing Company's, Oxford
14. Grosse CU, Reinhardt HW, Finck F (2003) Signal-based acoustic emission techniques in civil engineering. ASCE J Mater Civil Eng 15:274–279
15. Carpinteri A, Lacidogna G (2002) System for the assessment of safety conditions in reinforced concrete and masonry structures. Italian Patent No. To 2002 A000924, registered on 23 October 2002
16. Shah SP, Li Z (1994) Localization of microcracking in concrete under uniaxial tension. ACI Mater J 91: 372–381
17. Shcherbakov R, Turcotte DL (2003) Damage and self-similarity in fracture. Theor Appl Fract Mech 39: 245–258
18. Hollaway LC, Leeming MB (eds) (1999) Strengthening of reinforced concrete structures. Woodhead Publishing, Cambridge, England
19. Shigeishi M, Ohtsu M (2001) Acoustic emission moment tensor analysis: development for crack identification in concrete materials. Construct Build Mater 15:311–319
20. Chang SH, Lee CI (2004) Estimation of cracking and damage mechanisms in rock under triaxial compression by moment tensor analysis of acoustic emission. Int J Rock Mech Min Sci 41:1069–1086
21. Schubert F, Schechinger B (2002) Numerical modelling of acoustic emission sources and wave propagation in concrete. NDT.net, the e-J Nondestruct Test 7 (9)
22. Carpinteri A, Lacidogna G, Niccolini G (2006) Critical behaviour in concrete structures and damage localization by acoustic emission. Key Eng Mater (in press)
23. Lockner DA, Byerlee JD, Kuksenko V, Ponomarev A, Sidorin A (1991) Quasi-static fault growth and shear fracture energy in granite. Nature 350:39–42
24. ACI 440R-96 (1996) State-of-the-art report on fiber reinforced plastic (FRP). Reinforcement for concrete structures. American Concrete Institute (ACI), Committee 440, Michigan, USA
25. *fib* Bulletin (2001) Design and use of externally bonded FRP reinforcement (FRP EBR) for reinforced concrete structures. Bulletin no. 14, prepared by subgroup EBR (Externally Bonded Reinforcement) of *fib* Task Group 9.3 FRP Reinforcement for Concrete Structures
26. JCI (2003) Technical report on retrofitting technology for concrete structures. Technical Committee on Retrofitting Technology for Concrete Structures, pp 79–97
27. Ferretti D, Savoia M (2003) Cracking evolution in R/C members strengthened by FRP-plates. Eng Fract Mech 70:1069–1087
28. Ko H, Sato Y (2004) Analysis of FRP-strengthened concrete members with varied sheet bond stress-slip models. J Adv Conc Technol 2:317–326

29. Antonaci P, Bocca P (2005) On the non-destructive evaluation of the Young's modulus of concrete. In: Proc. of the 11th International Conference on Fracture, Turin, Italy
30. David E, Djelal C, Buyle-Bodin F (1998) Repair and strengthening of reinforced concrete beams using composite materials. In: Proc. of the 2nd international PhD symposium in civil engineering, Budapest
31. David E, Ragneau E, Buyle-Bodin F (2003) Experimental analysis of flexural behaviour of externally bonded CFRP reinforced concrete structures. Mater Struct 36:238–241
32. Carpinteri A (1989) Cusp catastrophe interpretation of fracture instability. J Mech Phys Solids 37:567–582
33. Uomoto T (1987) Application of acoustic emission to the field of concrete engineering. J Acoust Emission 6:137–144
34. Colombo S, Main IG, Forde MC (2003) Assessing damage of reinforced concrete beam using *b*-value analysis of acoustic emission signals. ASCE J Mater Civil Eng 15:280–286